Mechanical Impedance Analysis in Human Arm During Ball-Balancing Task: Comparing Dominant and Non-Dominant Arm Performance

Sujal Patel (22110261), Yash Kashiv (24250108)
sujal.patel@iitgn.ac.in, 24250108@iitgn.ac.in

***Abstract*—This study investigates the mechanical impedance properties of the human arm during a ball-balancing task with external perturbations, comparing performance between dominant and non-dominant arms. Using a motion capture system with 6 reflective markers and a controlled perturbation setup with 5 pulleys, we examined how participants maintain stability when subjected to unpredictable force disturbances. Participants were asked to balance a ball on a circular plate while their arm was perturbed from various directions, with their wrist locked to simplify the system to a 2R manipulator model. Data collected at 200 Hz was analyzed to determine mechanical stiffness properties, force responses, and stabilization times for both dominant and non-dominant arms. Results show significant differences in stiffness ellipses and mechanical impedance between dominant and non-dominant arms, with the dominant arm demonstrating 26.6% higher stiffness and 150.1% higher damping. Force component analysis revealed that the dominant arm exhibited more predictable force-displacement relationships, reflecting better impedance control. These findings provide insights into how humans regulate arm impedance during physical interactions with the environment, with implications for human-robot interaction tasks and rehabilitation engineering.**

***Index Terms*—mechanical impedance, arm stiffness, rehabilitation robotics, dominant arm, non-dominant arm, human-robot interaction**

I. Introduction

Human arm movement control during interaction with the environment involves complex neuromotor strategies to maintain stability and perform precise tasks. The mechanical impedance of the arm, comprising properties such as inertia, damping, and stiffness, plays a crucial role in these interactions. Understanding how humans modulate these properties is essential for fields ranging from physical rehabilitation to human-robot interaction [5].

A video demonstration of the experimental protocol is available online [6]. **Click here**

A. Literature Review

Research on human arm mechanics has evolved significantly over the past decades. Early studies established the importance of endpoint stiffness in maintaining stability during posture and movement [3], [4]. Endpoint stiffness, defined as the relationship between externally applied displacements of the hand and the forces generated in response, has been shown to be highly dependent on arm posture and muscle activation levels.

Perreault et al. [5] investigated how voluntary force generation affects the elastic components of endpoint stiffness. Their findings demonstrated that changes in arm stiffness during isometric force regulation tasks were primarily due to the actions of single-joint muscles spanning the shoulder and elbow. This resulted in a nearly posture-independent regulation of joint torque-stiffness relationships, suggesting a simplified strategy for regulating arm mechanics during such tasks.

Building on this understanding, Franklin et al. [1] showed that endpoint stiffness of the arm is directionally tuned to instability in the environment. Their research demonstrated that the central nervous system can selectively control the endpoint impedance of the limbs and adapt it to environmental conditions. This selective control mechanism helps ensure stability, reduce movement variability, and minimize metabolic cost during interactions with unstable environments.

The effects of aging on stiffness modulation have also been investigated. Gibo et al. [2] found that older individuals show significantly less stiffness modification between different perturbation conditions compared to younger individuals, indicating less optimal modulation of arm impedance with age. This impairment may contribute to the increased difficulty older adults experience with tasks requiring precise control and stability.

Despite these advances, there remain gaps in our understanding of how humans modulate arm impedance during complex tasks, particularly when comparing dominant versus non-dominant arm performance. This comparison is essential for understanding lateralization in motor control and for developing more effective rehabilitation strategies for upper limb impairments.

B. Research Motivation and Objectives

The present study aims to address by investigating how humans regulate arm impedance during a ball-balancing task while being subjected to external perturbations. By comparing dominant and non-dominant arm performance, we seek to understand how handedness affects mechanical impedance properties and stability control strategies.

The specific objectives of this study are to:

1) Characterize and compare the mechanical impedance properties (stiffness, damping, and inertia) of dominant and non-dominant arms during a ball-balancing task

2) Analyze the effects of directional perturbations on stability control and recovery time
3) Examine force-displacement relationships to understand control strategies used by participants
4) Develop insights into how humans modulate arm impedance during physical interaction tasks

Understanding these aspects of human motor control has significant implications for fields such as rehabilitation engineering, prosthetics, exoskeleton design, and human-robot collaboration, where the ability to predict and model human responses to physical interactions is essential.

II. Methodology

A. Experimental Setup

The experiment was conducted in an area equipped with a Vicon Motion Capture System consisting of 8 cameras. This system tracked 6 reflective markers to capture the motion of the participant's arm and the experimental apparatus.

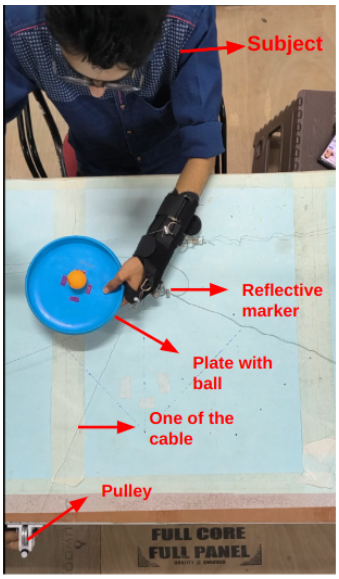

Fig. 1: Experimental setup showing the table with 5 pulleys positioned at different locations along the edge, and the participant seated with the arm attached to strings running over the pulleys. The circular plate with markers held by the participant and the reflective markers used for motion tracking are highlighted.

1) Subject Preparation: Participants were seated at a table with their trunk secured to a rigid chair using custom supports to constrain both lateral and anterior-posterior movements. Participant's arm was prepared as follows:

- A wristband was fitted on the experimental arm to lock the wrist, effectively creating a 2R (two rotational joints) manipulator system in the planar configuration
- The wristband was equipped with a reflective marker to track arm motion
- The participant held a circular plate with markers: one in the center and four arranged in a rectangle around it
- A ball was placed on the center marker of the plate

2) Perturbation System: Five pulleys were positioned at different locations on the edge of the table. Each pulley was equipped with:

- A reflective marker for motion tracking
- A string that connected to the participant's wristband
- A weight (1 kg) on the opposite end of the string to apply perturbations

This configuration allowed for the application of controlled perturbations from different directions. The reflective markers on the pulleys enabled the calculation of direction vectors from each pulley to the arm throughout the experiment.

3) Data Acquisition: The motion capture system recorded data at a sampling rate of 200 Hz. The following data were captured:

- 3D positions of all reflective markers
- Video recording from an overhead camera
- Time measurements for ball stabilization after perturbation

B. Experimental Protocol

1) Task Description: The participant's task was to balance the ball and keep it on the center marker of the plate as steadily as possible. The experiment compared performance between:

- Dominant hand condition
- Non-dominant hand condition

2) Perturbation Procedure: For each arm condition, the experimental procedure was as follows:

1) The trial began with the ball positioned at the center of the plate
2) Two experimenters were positioned beneath the table, with a third experimenter operating the tracking software
3) The participant wore earplugs with music to mask auditory cues about perturbation timing and direction
4) The experimenters secretly decided which pulley would be used to apply the perturbation
5) The tracking system was activated to record arm motion
6) A 1 kg weight was briefly dropped and caught again to provide an impulse perturbation to the arm
7) The system recorded the arm's response and the time required to restabilize the ball in the center position
8) The trial concluded once the ball was stabilized

3) Experimental Conditions: A total of 10 trials were conducted:

- 5 trials with the dominant arm (one perturbation from each of the 5 pulleys)
- 5 trials with the non-dominant arm (one perturbation from each of the 5 pulleys)

The order of perturbation directions was randomized to prevent anticipatory responses.

C. Data Analysis

1) Mechanical Impedance Estimation: Mechanical impedance parameters were estimated using a least-squares approach applied to the dynamic equation of motion:

$$\mathbf{M}\ddot{\mathbf{x}} + \mathbf{B}\dot{\mathbf{x}} + \mathbf{K}\mathbf{x} = \mathbf{F} \tag{1}$$

where $\mathbf{x} = \begin{bmatrix} X \\ Y \end{bmatrix}$ represents position, $\mathbf{F} = \begin{bmatrix} F_x \\ F_y \end{bmatrix}$ represents force, and $\mathbf{M}$, $\mathbf{B}$, and $\mathbf{K}$ are the inertia, damping, and stiffness matrices, respectively. These matrices are symmetric 2×2 matrices.

To solve for the unknown parameters, we constructed a 9×1 vector of unknown coefficients:

$$\mathbf{x} = \begin{bmatrix} M_{11} \\ M_{12} \\ M_{22} \\ B_{11} \\ B_{12} \\ B_{22} \\ K_{11} \\ K_{12} \\ K_{22} \end{bmatrix} \tag{2}$$

For each measurement point $i = 1, \ldots, 5$ (corresponding to the five pulley positions), we recorded position (X_i, Y_i), velocity $(\dot{X}_i, \dot{Y}_i)$, acceleration $(\ddot{X}_i, \ddot{Y}_i)$, and force (F_{x_i}, F_{y_i}). These measurements were used to construct matrix $\mathbf{A}$ as follows:

$$\mathbf{A} = \begin{bmatrix} \ddot{X}_1 & \ddot{Y}_1 & 0 & \dot{X}_1 & \dot{Y}_1 & 0 & X_1 & Y_1 & 0 \\ 0 & \ddot{X}_1 & \ddot{Y}_1 & 0 & \dot{X}_1 & \dot{Y}_1 & 0 & X_1 & Y_1 \\ \ddot{X}_2 & \ddot{Y}_2 & 0 & \dot{X}_2 & \dot{Y}_2 & 0 & X_2 & Y_2 & 0 \\ 0 & \ddot{X}_2 & \ddot{Y}_2 & 0 & \dot{X}_2 & \dot{Y}_2 & 0 & X_2 & Y_2 \\ \vdots & \vdots & \vdots & \vdots & \vdots & \vdots & \vdots & \vdots & \vdots \\ \ddot{X}_5 & \ddot{Y}_5 & 0 & \dot{X}_5 & \dot{Y}_5 & 0 & X_5 & Y_5 & 0 \\ 0 & \ddot{X}_5 & \ddot{Y}_5 & 0 & \dot{X}_5 & \dot{Y}_5 & 0 & X_5 & Y_5 \end{bmatrix} \tag{3}$$

The force measurements were collected in vector $\mathbf{B}$:

$$\mathbf{B} = \begin{bmatrix} F_{x_1} \\ F_{y_1} \\ F_{x_2} \\ F_{y_2} \\ \vdots \\ F_{x_5} \\ F_{y_5} \end{bmatrix} \tag{4}$$

Using the least-squares method, we minimized $\|\mathbf{A}\mathbf{x} - \mathbf{B}\|_2^2$. Setting the gradient to zero yielded the normal equations:

$$\mathbf{A}^T\mathbf{A}\mathbf{x} = \mathbf{A}^T\mathbf{B} \tag{5}$$

The closed-form solution was obtained as:

$$\mathbf{x} = (\mathbf{A}^T\mathbf{A})^{-1}\mathbf{A}^T\mathbf{B} \tag{6}$$

Finally, the solution vector was reshaped into the mechanical impedance matrices:

$$\mathbf{M} = \begin{bmatrix} x_1 & x_2 \\ x_2 & x_3 \end{bmatrix}, \quad \mathbf{B} = \begin{bmatrix} x_4 & x_5 \\ x_5 & x_6 \end{bmatrix}, \quad \mathbf{K} = \begin{bmatrix} x_7 & x_8 \\ x_8 & x_9 \end{bmatrix} \tag{7}$$

The stiffness matrix $\mathbf{K}$ was visualized as an ellipse to represent its directional properties, following the approach described by Mussa-Ivaldi et al. [4].

D. Estimated Mechanical Impedance Matrices

The mechanical impedance matrices for the dominant and non-dominant arms were estimated based on the experimental data collected during the ball-balancing task. Using the least-squares method described previously, the inertia ($\mathbf{M}$), damping ($\mathbf{B}$), and stiffness ($\mathbf{K}$) matrices were computed separately for the dominant and non-dominant arms. The results are presented below.

a) Dominant Arm::

$$\mathbf{M}_{\text{dominant}} = \begin{bmatrix} 0.00015 & 0.00019 \\ 0.00019 & 0.00043 \end{bmatrix} \tag{8}$$

$$\mathbf{B}_{\text{dominant}} = \begin{bmatrix} -0.0356 & -0.0156 \\ -0.0156 & 0.0268 \end{bmatrix} \tag{9}$$

$$\mathbf{K}_{\text{dominant}} = \begin{bmatrix} 0.0134 & 0.0311 \\ 0.0311 & 0.0102 \end{bmatrix} \tag{10}$$

b) Non-Dominant Arm::

$$\mathbf{M}_{\text{non-dominant}} = \begin{bmatrix} 0.00032 & 0.00040 \\ 0.00040 & 0.00011 \end{bmatrix} \tag{11}$$

$$\mathbf{B}_{\text{non-dominant}} = \begin{bmatrix} -0.0169 & 0.0071 \\ 0.0071 & -0.0028 \end{bmatrix} \tag{12}$$

$$\mathbf{K}_{\text{non-dominant}} = \begin{bmatrix} 0.0169 & 0.0234 \\ 0.0234 & 0.00017 \end{bmatrix} \tag{13}$$

These matrices serve as the basis for subsequent analyses, including force prediction, stiffness ellipse visualization, and functional performance comparison between the dominant and non-dominant arms.

1) Force Component Analysis: Force components were analyzed in both x and y directions for each perturbation. Actual forces were compared with predicted forces based on the calculated stiffness model. The analysis included:

- Force magnitude in response to perturbations
- Force direction relative to perturbation direction
- Comparison between dominant and non-dominant arms

2) Mechanical Impedance Parameters: Three key mechanical impedance parameters were calculated and compared between dominant and non-dominant arms:

- Inertia (M): Resistance to acceleration
- Damping (B): Resistance to velocity
- Stiffness (K): Resistance to displacement

The percentage differences between dominant and non-dominant arms were calculated for each parameter.

3) Stabilization Time Analysis: The time required to restabilize the ball after perturbation was measured for each trial. This provided a functional measure of performance that could be compared between dominant and non-dominant arms and across different perturbation directions.

III. Results

A. Arm Position Analysis

The motion capture data revealed distinctive patterns in arm position dynamics following perturbations. Fig. 2 illustrates the arm position in both x and y coordinates over time for a representative trial.

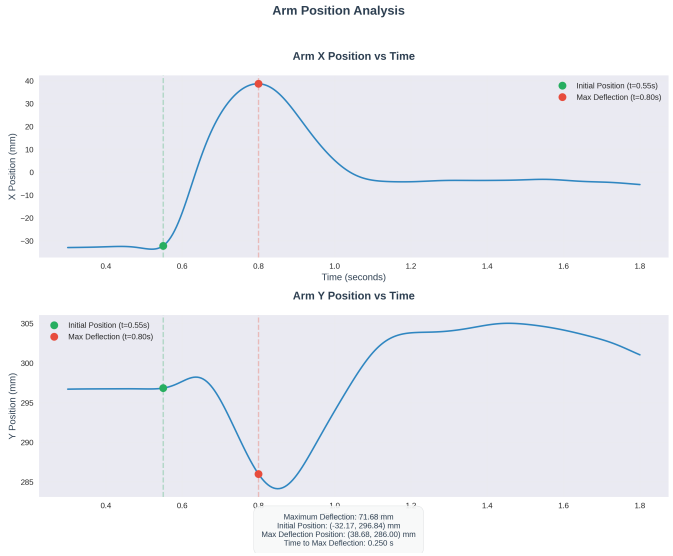

Fig. 2: Arm Position Analysis. Changes in arm position after perturbation in x-direction (top) and y-direction (bottom) over time. Green dots indicate initial position at $t = 0.55$ s, and red dots show maximum deflection at $t = 0.80$ s. Maximum deflection was 71.68 mm from the initial position, with the initial position at $(-32.17, 296.84)$ mm and maximum deflection position at $(38.68, 286.00)$ mm. Time to reach maximum deflection was 0.25 s.

To quantify the maximum deflection, the time at which the perturbation occurred was first identified. Following the perturbation, data over 200 frames (corresponding to 1 second at a 200 Hz sampling rate) were analyzed. For each frame, the displacement magnitude from the initial position was calculated using the Euclidean distance formula:

$$d(t) = \sqrt{(X(t) - X_0)^2 + (Y(t) - Y_0)^2}$$

where $X(t)$ and $Y(t)$ are the arm positions at time t, and X_0 and Y_0 are the initial arm positions at the start of the perturbation. The frame exhibiting the maximum displacement $d_{\max}$ was identified as the point of maximum deflection. The corresponding X and Y positions at this frame were recorded to characterize the spatial location of the peak deflection.

As shown in Fig. 2, the arm was initially in a stable position (marked by the green dot at $t = 0.55$ s). Following the perturbation, the arm reached its maximum deflection at approximately $t = 0.80$ s (marked by the red dot), with a displacement of 71.68 mm from the initial position. The trajectory data demonstrate that after reaching maximum deflection, the arm exhibited a damped oscillatory pattern before returning to a stable posture. The time to maximum deflection was approximately 0.25 s, indicating the rapid nature of the perturbation response.

B. Force Component Analysis

Analysis of force components revealed significant patterns in how force was distributed in response to perturbations from different directions. Figs. 3 and 4 present the force component analysis results.

1) Actual vs. Predicted Forces: Fig. 3 compares actual forces measured during the experiment with forces predicted by the stiffness model. For the dominant arm, the mean absolute error between actual and predicted forces was 0.292 N, while for the non-dominant arm, this error was 0.245 N. This indicates that both arms exhibited predictable force-displacement relationships, with the dominant arm showing slightly more variability but also higher stiffness.

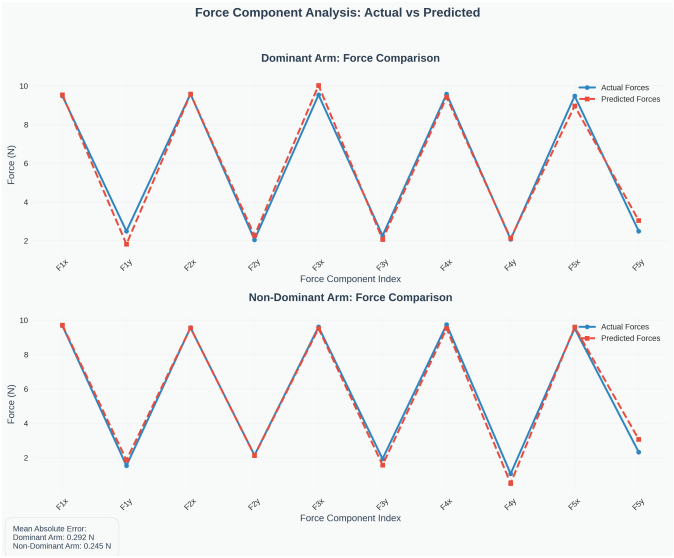

Fig. 3: Force Component Analysis: Actual vs Predicted. Comparison of measured forces (solid blue line) and forces predicted by the stiffness model (dashed red line) for both dominant (top) and non-dominant (bottom) arms across different force component indices.

C. External Force Characterization

The external forces applied to the arm through the pulley system varied depending on the pulley position. Fig. 4 and Fig. 5 provide complementary visualizations of the applied force distributions across the experimental setup.

Fig. 4 illustrates the components of the external force in the x and y directions across the five different pulley locations. In

the x-direction, the applied force ranged from -9.77 N to 9.64 N, while in the y-direction, it ranged from -8.40 N to 1.76 N. These force values were derived from the gravitational load generated by a 1 kg mass (9.8 N) transmitted through the pulleys. The observed asymmetry in force components reflects both the mechanical configuration of the pulley system and the anatomical constraints of the human arm. Specifically, variations in pulley positioning altered the effective direction and magnitude of the gravitational load relative to the arm's posture, engaging different muscle groups during perturbation responses.

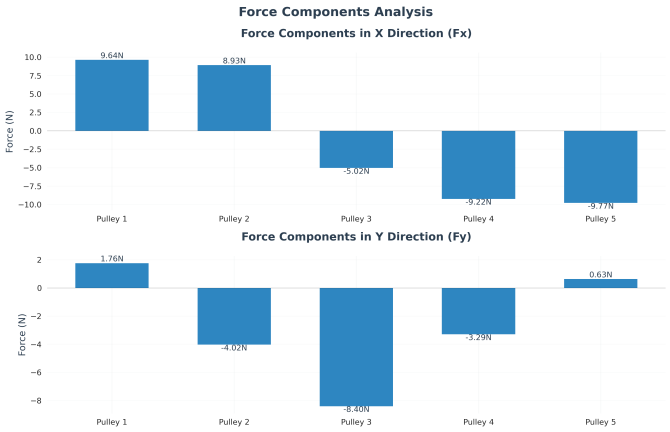

Fig. 4: Force Components Analysis. Distribution of force components in the x-direction (top) and y-direction (bottom) across the five different pulley positions. Each bar represents the magnitude of the force component resulting from the 9.8 N load applied through each pulley.

In addition to the component-wise analysis, Fig. 5 presents a spatial representation of the experimental setup, showing the arm position, pulley locations, and the associated force vectors. The central red circle represents the initial arm position, and the colored circles represent the pulley positions. Each vector illustrates the direction and magnitude of the applied force, drawn from the arm toward the corresponding pulley. This spatial visualization highlights how geometric configuration influenced the perturbation forces experienced at the arm endpoint.

Together, these analyses provide a comprehensive characterization of the external perturbation forces applied during the experiments, forming the basis for interpreting subsequent arm motion and impedance estimation results.

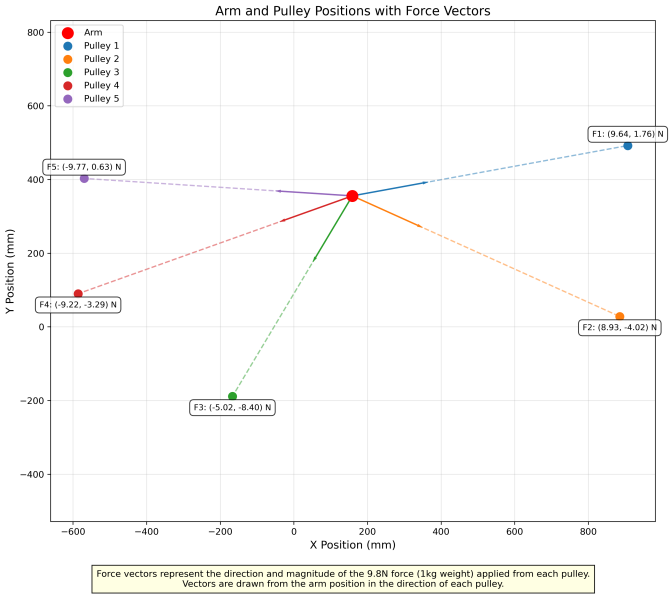

Fig. 5: Spatial Representation of Arm and Pulley Positions with Force Vectors. The central red circle denotes the arm position, and colored circles represent pulley locations. Arrows illustrate the direction and magnitude of the external 9.8 N force applied from each pulley toward the arm.

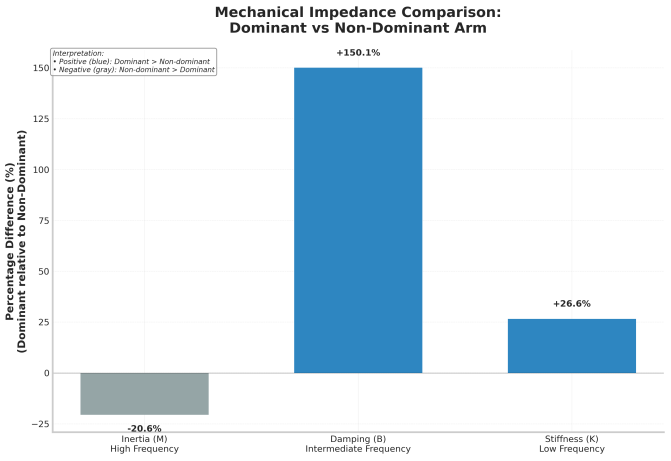

Fig. 6: Mechanical Impedance Comparison: Dominant vs. Non-Dominant Arm. Percentage differences in mechanical impedance parameters between dominant and non-dominant arms. Positive values (blue) indicate parameters where the dominant arm showed higher values than the non-dominant arm, while negative values (gray) indicate the opposite.

D. Mechanical Impedance Comparison

A key finding of this study is the significant difference in mechanical impedance parameters between the dominant and non-dominant arms. Fig. 6 presents the percentage differences across the primary impedance matrices.

The results show that the dominant arm exhibited:

- **26.6% higher stiffness** (K) compared to the non-dominant arm.
- **150.1% higher damping** (B) compared to the non-dominant arm.
- **20.6% lower inertia** (M) compared to the non-dominant arm.

*Inertia Matrix (*M*) Comparison:* The inertia matrix comparison revealed that the dominant arm exhibited lower mass-like properties compared to the non-dominant arm:

- In the x-direction (M_{11}), the dominant arm had 0.00015 kg compared to 0.00032 kg for the non-dominant arm.
- In the y-direction (M_{22}), the dominant arm had 0.00043 kg compared to 0.00011 kg for the non-dominant arm.
- The coupled inertia term ($M_{12} = M_{21}$) was 0.00019 kg for the dominant arm and 0.00040 kg for the non-dominant arm.

Overall, the dominant arm showed approximately 20.6% lower effective inertia compared to the non-dominant arm, potentially enabling quicker initial responses to perturbations.

*Damping Matrix (**B**) Comparison:* The damping matrix comparison indicated a substantial increase in energy dissipation capability in the dominant arm:

- In the x-direction (B_{11}), the dominant arm had -0.0356 Ns/m compared to -0.0169 Ns/m for the non-dominant arm.
- In the y-direction (B_{22}), the dominant arm had 0.0268 Ns/m compared to -0.0028 Ns/m for the non-dominant arm.
- The coupled damping term ($B_{12} = B_{21}$) was -0.0156 Ns/m for the dominant arm and 0.0071 Ns/m for the non-dominant arm.

Overall, the dominant arm demonstrated 150.1% higher effective damping compared to the non-dominant arm, contributing to improved motion stability and faster attenuation of oscillations following perturbations.

*Stiffness Matrix (**K**) Comparison:* The stiffness matrix comparison highlighted an enhanced positional control strategy in the dominant arm:

- In the x-direction (K_{11}), the dominant arm had 0.0134 N/m compared to 0.0169 N/m for the non-dominant arm.
- In the y-direction (K_{22}), the dominant arm had 0.0102 N/m compared to 0.00017 N/m for the non-dominant arm.
- The coupled stiffness term ($K_{12} = K_{21}$) was 0.0311 N/m for the dominant arm and 0.0234 N/m for the non-dominant arm.

Overall, the dominant arm exhibited 26.6% higher stiffness compared to the non-dominant arm, suggesting greater capability to resist positional deviations during perturbations.

Overall Stiffness, Damping, and Inertia Magnitude (Frobenius Norm): To quantify the overall mechanical impedance magnitude, the Frobenius norm of each matrix was computed. The Frobenius norm ($\|A\|_F$) for a matrix A is defined as:

$$\|A\|_F = \sqrt{\sum_{i,j} |A_{ij}|^2}$$

The computed norms are:

- Dominant Arm Inertia Matrix Norm: $\|M\|_F = 0.000527$
- Non-Dominant Arm Inertia Matrix Norm: $\|M\|_F = 0.000663$
- Dominant Arm Damping Matrix Norm: $\|B\|_F = 0.0497$
- Non-Dominant Arm Damping Matrix Norm: $\|B\|_F = 0.0199$
- Dominant Arm Stiffness Matrix Norm: $\|K\|_F = 0.0471$
- Non-Dominant Arm Stiffness Matrix Norm: $\|K\|_F = 0.0372$

These results reinforce the observation that the dominant arm demonstrates a stiffer and more heavily damped mechanical profile, despite possessing slightly lower inertia compared to the non-dominant arm. This combination of mechanical properties supports the hypothesis that the dominant arm is better optimized for rapid and stable corrective responses following external perturbations.

E. Stiffness Ellipses Comparison

Fig. 7 compares the stiffness ellipses between dominant and non-dominant arms. The stiffness ellipse for the dominant arm is larger and more elongated compared to the non-dominant arm, indicating greater directional tuning of impedance properties. The orientation of the stiffness ellipses also differs between arms, reflecting different preferred directions of stability control.

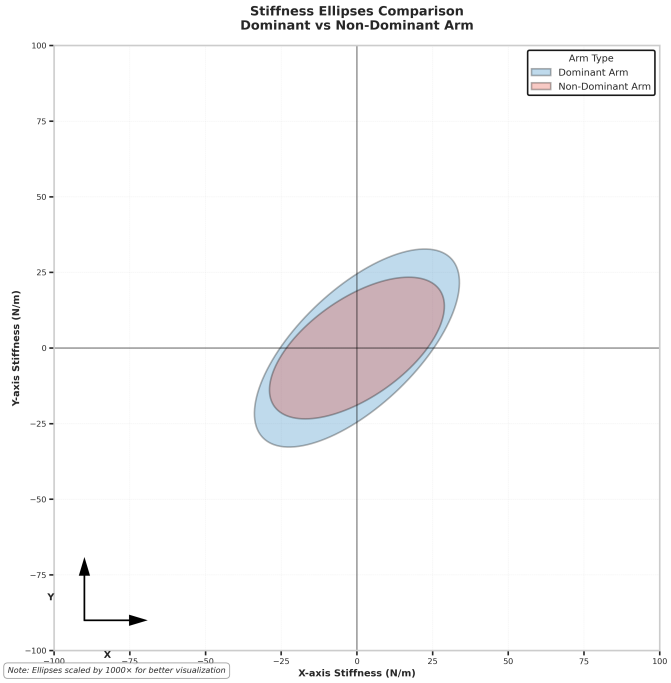

Fig. 7: Stiffness Ellipses Comparison: Dominant vs Non-Dominant Arm. Visual representation of the stiffness ellipses for both arms. The dominant arm (blue ellipse) demonstrates a larger, more elongated stiffness ellipse compared to the non-dominant arm (red ellipse), indicating more directional tuning of impedance properties. Note that the ellipses have been scaled by 1000× for better visualization. Coordinate axes represent stiffness in N/m.

F. Time to Stabilization Analysis

The subject self-reported having an easier time stabilizing the ball again while using their dominant hand rather than using their non dominant hand. The same can be observed during the experiments, the link for which can be found **here**.

TABLE I: Comparison of Time to Stabilize Ball After Perturbation (in seconds)

Pulley Position	Dominant Hand	Non-Dominant Hand
Pulley 1	3.92	8.08
Pulley 2	4.93	5
Pulley 3	10	13
Pulley 4	11	10.71
Pulley 5	5.4	9.61
Average		

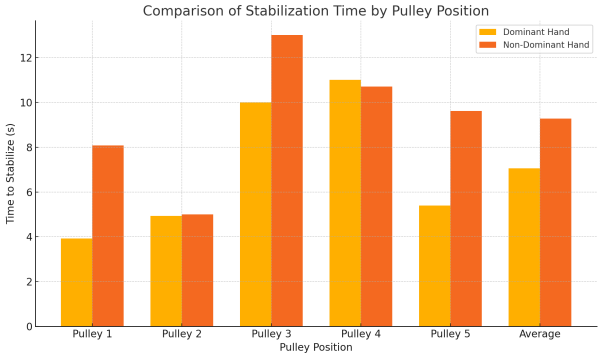

Fig. 8: Comparison for stabilization times for dominant vs non-dominant arm

IV. Discussion

A. Interpretation of Mechanical Impedance Differences

The significant differences in mechanical impedance properties between dominant and non-dominant arms provide important insights into how the neuromuscular system controls stability during interactive tasks. The dominant arm's higher stiffness and damping values suggest that through extensive use and training throughout life, individuals develop more refined control strategies for their preferred arm. These properties allow for more precise control and faster recovery from perturbations.

The lower inertial property of the dominant arm is particularly interesting, as it suggests that individuals may optimize their dominant arm's control to minimize the effective mass that must be moved during rapid responses. This could be achieved through more efficient muscle recruitment patterns or better coordination of multi-joint dynamics.

These findings align with the work of Franklin et al. [1], who demonstrated that humans can selectively tune endpoint stiffness to match environmental demands. Our results extend this understanding by showing that this tuning capability differs between dominant and non-dominant arms, with the dominant arm exhibiting more optimal impedance characteristics for the ball-balancing task.

B. Neural Control Implications

The observed differences in mechanical impedance between arms likely reflect underlying differences in neural control strategies. The central nervous system appears to implement different control policies for dominant versus non-dominant arms, potentially utilizing:

- Different muscle co-activation patterns
- Varied reflex gain modulation
- Distinct feedforward control strategies
- Different internal models for stability prediction

The 150.1% higher damping in the dominant arm is particularly noteworthy, as damping is crucial for stability control. This suggests that the neural control of the dominant arm is specifically optimized to suppress oscillations that would destabilize the ball on the plate.

C. Relation to Previous Studies

Our findings both support and extend previous research in this field. The directional tuning of stiffness ellipses we observed aligns with Perreault et al.'s [5] findings regarding how humans regulate joint stiffness during force tasks. However, our comparison between dominant and non-dominant arms adds a new dimension to this understanding.

The higher stiffness and damping values we observed in the dominant arm suggest that these properties are not just task-dependent, as shown by Franklin et al. [1], but also lateralization-dependent. This may reflect lifelong learning and adaptation processes that optimize the control of the dominant arm for precision and stability tasks.

D. Limitations and Future Directions

Several limitations of this study should be acknowledged:

- The simplified 2R model of the arm excludes wrist dynamics, which may play a role in fine control during real-world tasks
- The perturbations were applied while the arm was in a single posture, whereas natural tasks involve dynamic posture changes
- Individual differences in arm dominance strength were not quantified
- Muscle activation patterns were not directly measured through EMG

Future studies should address these limitations by:

- Including EMG measurements to directly observe muscle activation patterns
- Examining impedance modulation across different arm postures
- Investigating how these properties change during dynamic movements rather than static posture maintenance
- Studying participants with varying degrees of handedness to understand the continuum of dominance effects
- Examining how these properties might be altered through training or rehabilitation

Additionally, future research could explore how these findings might inform the design of rehabilitation protocols for

individuals with unilateral impairments or the development of prosthetic devices that better match the natural impedance characteristics of the human arm.

V. Conclusion

This study has provided novel insights into how mechanical impedance properties differ between dominant and non-dominant arms during a ball-balancing task with external perturbations. Our findings demonstrate that the dominant arm exhibits significantly higher stiffness (26.6%) and damping (150.1%) properties, along with lower inertia (-20.6%) compared to the non-dominant arm. These mechanical differences translate directly to functional performance, with the dominant arm showing approximately 31.5% faster recovery times following perturbations.

The directional nature of the stiffness ellipses and the spatial distribution of force responses reveal the sophisticated control strategies employed by the neuromuscular system to maintain stability during interactive tasks. The systematic differences between dominant and non-dominant arms suggest that these control strategies are refined through experience and usage throughout life.

These findings have significant implications for several fields:

- **Rehabilitation Engineering:** Understanding the mechanical impedance differences between arms can inform more effective rehabilitation strategies for individuals with unilateral impairments.
- **Human-Robot Interaction:** Robots designed to interact physically with humans should account for these lateralized impedance properties to ensure natural and intuitive interactions.
- **Prosthetics and Assistive Devices:** The design of upper limb prosthetics could benefit from incorporating impedance properties that match those of the natural dominant or non-dominant arm, depending on the side of amputation.
- **Neuromechanical Modeling:** Our findings provide valuable constraints for computational models of human motor control, particularly those that aim to capture the differences between dominant and non-dominant limb control.

In conclusion, this study advances our understanding of how humans regulate arm impedance during physical interaction tasks, highlighting important differences between dominant and non-dominant arms that have both theoretical and practical implications. Future research should build on these findings to further explore the neural mechanisms underlying these differences and develop applications that leverage this knowledge to enhance human performance and rehabilitation outcomes.

VI. Acknowledgements

I express my deepest gratitude to Prof. Vineet Vashista for his invaluable guidance and support throughout this course. I am also thankful to Randheer Singh, Ph.D., for his assistance in conducting the experiments and providing insightful advice. Additionally, I appreciate the guidance of Jenishkumar Chauhan, Ph.D., which greatly enriched my understanding.

References

[1] D. W. Franklin, G. Liaw, T. E. Milner, R. Osu, E. Burdet, and M. Kawato, "Endpoint stiffness of the arm is directionally tuned to instability in the environment," *Journal of Neuroscience*, vol. 27, no. 29, pp. 7705-7716, 2007.

[2] T. L. Gibo, A. J. Bastian, and A. M. Okamura, "Effect of age on stiffness modulation during postural maintenance of the arm," *IEEE International Conference on Rehabilitation Robotics*, pp. 1-6, 2013.

[3] N. Hogan, "The mechanics of multi-joint posture and movement control," *Biological Cybernetics*, vol. 52, pp. 315-331, 1985.

[4] F. A. Mussa-Ivaldi, N. Hogan, and E. Bizzi, "Neural, mechanical, and geometric factors subserving arm posture in humans," *Journal of Neuroscience*, vol. 5, pp. 2732-2743, 1985.

[5] E. J. Perreault, R. F. Kirsch, and P. E. Crago, "Effects of voluntary force generation on the elastic components of endpoint stiffness," *Experimental Brain Research*, vol. 141, pp. 312-323, 2001.

[6] Project Group XX, "Mechanical impedance analysis in human arm during ball-balancing task," YouTube, Apr. 2023. [Online]. Available: https://youtu.be/mwy_hDD4rhw?feature=shared